**The neuronal ceroid lipofuscinosis protein, Cln7, regulates neural development from the post-synaptic cell.**

Megan B. O'Hare* [1], Alamin Mohammed* [2], Kyle J. Connolly[2], Katelyn M. Aitchison[2], Niki C. Anthoney[2], Amy L. Roberts[2], Matthew J. Taylor [2], Bryan A. Stewart[3,4], Richard I. Tuxworth# [1,2] and Guy Tear# [1]

1: Department of Developmental Neurobiology
King's College London
New Hunt's House
London
SE1 1UL
UK

2: Institute of Cancer and Genomic Sciences
University of Birmingham
Birmingham
B15 2TT
UK

3: Department of Biology
University of Toronto Mississauga
Mississauga, ON
L5L 1C6
Canada

4. Department of Cell and Systems Biology
University of Toronto
Toronto, ON
M5S 3G5
Canada

* Equal contribution

# Joint correspondence:
Guy.Tear@kcl.ac.uk
+44 (0)20 7848 6539

R.I.Tuxworth@bham.ac.uk
+44 (0)121 414 7046

**ORCIDs:**

MJT: 0000-0003-3055-4453
NCA: 0000-0003-3311-6328
KJC: 0000-0003-2425-3910
BAS: 0000-0003-2520-3632
RIT: 0000-0001-5697-6254
GT: 0000-0002-3114-7537

**Running Title:**
Cln7 regulates neural development

**Key words:**
Neuronal ceroid lipofuscinosis, NCL, Cln7, retrograde signaling, neuromuscular junction, NMJ, *Drosophila*

**Summary**

Cln7, a protein disrupted in an early-onset neurodegenerative disease, is required for normal development of the Drosophila neuromuscular junction. Cln7 functions by regulating TORC signaling in the post-synaptic muscle as part of trans-synaptic communication that matches pre- and post-synaptic development.

**Abstract**

The neuronal ceroid lipofuscinoses (NCLs) are a group of monogenetic neurodegenerative disorders with an early onset in infancy or childhood. Despite identification of the genes disrupted in each form of the disease, their normal cellular role and how their deficits lead to disease pathology is not fully understood. Cln7, a major facilitator superfamily domain-containing protein, is affected in a late infantile-onset form of NCL. We demonstrate that in *Drosophila,* Cln7 is required for normal synapse development. In the absence of Cln7 the neuromuscular junction fails to develop fully leading to reduced function and behavioral changes. Cln7 is required in the post-synaptic muscle for appropriate pre-synaptic development suggesting an involvement in regulating trans-synaptic communication. Loss of Cln7 leads to reduced TORC activity, suggesting Cln7 acts as a regulator of TORC activity to influence synaptic development.

## Introduction

The study of early-onset, inherited forms of neurodegenerative disease provides an opportunity to identify how single gene defects lead to neurodegeneration. The neuronal ceroid lipofuscinoses (NCLs) are a group of such monogenetic neurodegenerative disorders with disease onset early in infancy or childhood (5-8 years in the most common form but congenital and rare adult-onset forms also exist). Patients present with a loss of visual acuity followed by onset of seizures and psychiatric disturbances. A progressive mental decline follows, accompanied by loss of motor skills and death usually occurs by the age of 20-30 (Jalanko and Braulke, 2009). The NCLs share a hallmark pathology: accumulation of fluorescent storage material indicating lysosomal dysfunction. The progression of NCL pathology appears similar to many other neurodegenerative disorders in that changes to synapses occur very early and a local activation of glia precedes a regionally specific loss of neurons (Kielar et al., 2009; Koch et al., 2011). Their early onset may well indicate that one or more key cellular pathways are impaired directly, rather than a consequence of the progressive buildup of factors as may occur in the late-onset diseases. There is also likely to be a significant developmental component to the neuropathology, potentially pre-disposing the nervous system to degeneration.

The NCLs are recessively inherited monogenic disorders (with the exception of one rare adult-onset autosomal dominant form) and mutations have been identified in 14 genes responsible for NCL with varying ages of onset. A limited set of these genes is conserved in *Drosophila* suggesting that they are performing core functions necessary for normal neuronal health. Mutations in *CLN7/MFS-domain containing 8* (*CLN7*/*MFSD8*) are responsible for late-infantile onset NCL (LINCL or CLN7 disease), with disease onset at 1.5-5 years of age (Kousi et al., 2009). The CLN7 protein is predicted to be a member of the multi-facilitator superfamily of transporters, each of which has twelve membrane spanning domains (Siintola et al., 2007). However, its function remains unknown with no information on binding partners or whether it has any transport activity. In cell culture experiments with tagged forms, CLN7 protein is localized primarily in lysosomes (Sharifi et al., 2010; Siintola et al., 2007; Steenhuis et al., 2010) and has been identified by lysosomal proteomics (Chapel et al., 2013). Consistent with this, phenotypes in mutant mice show lysosomal dysfunction and a potential impairment of autophagy (Brandenstein et al., 2016).

*Cln7* is expressed widely within the murine CNS with high mRNA expression in the cerebellum and hippocampus (Sharifi et al., 2010). A Cln7-lacZ reporter construct also reveals expression in the entire cerebral cortex, caudate putamen and thalamus. In the spinal cord Cln7 is expressed in the gray matter but excluded from white matter (Damme et al, 2014). We similarly find that *Drosophila* Cln7 is expressed in the CNS. However, using GFP-tagged Cln7 expressed from its endogenous locus, we observe that Cln7 is enriched in glial cells in the CNS (Mohammed et al, 2017). Cln7 is also expressed in the neuromuscular system where high levels are found in the postsynaptic muscles where, significantly, it concentrates at the post-synaptic density (PSD) of the neuromuscular junction.

Neurodevelopmental defects (unless severe) are difficult to identify in standard rodent models. We turned to the *Drosophila* neuromuscular junction (NMJ), which provides a simple, genetically tractable model system to study the development and maturation of neurons and the assembly and function of synapses. Many genes associated with human neurological conditions, including developmental disorders and neurodegenerative diseases, have roles regulating NMJ development (Charng et al., 2014; Sharifi et al., 2010). As the *Drosophila* larva proceeds through development, increasing 100-fold in volume over 3-days, the concomitant expansion of the NMJ is regulated by homeostatic processes to maintain the correct levels of innervation to the body wall muscles. Multiple cellular pathways mediate both short-term and longer-term homeostasis, acting at both sides of the synapse. These include a BMP-mediated retrograde signal from the post-synaptic muscle, and a TOR-based translational response and many of these mechanisms also act similarly to regulate homeostasis in mammalian neurons (Frank, 2014). In addition, normal autophagic flux and endo-lysosomal function are required to maintain the synapse with mutants affecting lysosomal function, including Spinster and the cation channel Trpml, and autophagy, including several of the *atg* mutants, impacting on NMJ development and expansion of the pre-synaptic compartment (Shen and Ganetzky, 2009; Sweeney and Davis, 2002; Wong et al., 2012), Evidence is building in several models that loss of the *CLN* genes impacts on synapse dysfunction suggesting that they play a common role either within neurons or non-neuronal cells to maintain the synapse (Aby et al., 2013; Grunewald et al., 2017; Kielar et al., 2009; Partanen et al., 2008).

To study a potential role for Cln7 in neural development, we generated a *Drosophila* model for CLN7 disease by deleting the N-terminal half of the *Cln7* gene. While the animals

remain viable, they display impaired locomotion and an associated reduction in synapse size and altered synapse function. We show autophagy and retrograde BMP signaling are largely intact in Cln7 mutants and instead the neurodevelopmental defect may be due to changes in TOR complex activity in the post-synaptic cell. We demonstrate phenotypes consistent with a failure to activate TOR and an interaction between Cln7 and the TOR activating protein, Rheb. Finally, we demonstrate that in mammalian cells, activation of TOR is similarly compromised by loss of Cln7. This places Cln7 as a novel regulator of TORC activity and highlights the importance of this pathway in neural development and disease.

## Results

### Generation of a *Drosophila* model of CLN7 disease

Disruption of the *Mfsd8/Cln7* gene has been identified as the cause of the LINCL form of the NCLs (Kousi et al., 2009). Subsequently, more than 30 different *Cln7* mutations have been characterized. The *Drosophila* gene CG8596 shows 57% amino acid homology to human Cln7 and is likely to be the unique *Drosophila* orthologue of *Cln7*. The gene encodes a predicted 12-spanning transmembrane protein that has strong sequence homology to the multifacilitator family of solute transporters (Muzaffar and Pearce, 2008) (Fig. 1A). To study the functional role of Cln7, we generated two loss-of-function alleles of *Cln7* by imprecise excision of the P-element NP0345 inserted in the 5' UTR upstream of the start codon (Figure 1B). Two alleles were generated. Exons 1-5 were excised in the $Cln7^{84D}$ allele, with some P-element sequence remaining and exons 1 and 2 and part of exon 3 were excised in $Cln7^{36H}$ (Fig. 1B). Both mutant alleles are viable and fertile when homozygous, and show no developmental delay.

### Cln7 is required for normal synapse development

In a parallel study we generated Venus-YFP knock-in forms of Cln7 by CRISPR/Cas9-mediated gene editing to act as a reporter of expression and sub-cellular localization (Mohammed et al, 2017). Surprisingly, we identified that Cln7 is primarily a glial protein in the CNS but is also expressed in the body wall muscles that form the post-synaptic cells of the neuromuscular junction (NMJ), where it concentrates at the post-synaptic density (PSD; Fig. 2A and see Mohammed et al, 2017). The *Drosophila* NMJ is a readily accessible glutamatergic synapse and an excellent model system to study synapse function, so this discovery afforded us an opportunity to ask how Cln7 might function at the PSD. The peripheral NMJs in late stage larvae are easily identifiable using immunofluorescence and the innervations are simple, with 2-4 individual motoneurons contacting each muscle cell. The type I motoneurons that innervate the muscle can be further subdivided into two classes called type Ib and type Is classified according to the size of the presynaptic terminal swellings known as boutons (Fig. 2B). The type Ib terminals provide tonic stimulation and

the type Is phasic (Lnenicka and Keshishian, 2000). The overall size of the NMJ is governed by intra-neuronal and trans-synaptic homeostatic mechanisms that modulate NMJ size during development to match pre-synapse size and strength to muscle size (Frank, 2014). Many mutations affecting the structural and electrical properties of the NMJ consequently affect its size at the late larval stage, including many mutations related to human neurological diseases (Charng et al., 2014). These may influence one of a number of cellular signaling pathways that co-operate to regulate NMJ development including BMP and signaling via the TOR complex (TORC).

We find that *Cln7*$^{-/-}$ animals have a reduced development of the NMJ. Manual counting of the swellings of the terminal (boutons) is commonly used as a simple measure of terminal size as the boutons contain most of the active zone synaptic vesicle release sites. At muscle 4 we see a significant reduction of the type Ib motoneuron terminals in the *Cln7* mutant larvae when compared to isogenic control larvae (Fig. 2C). Some of the boutons in the *Cln7* larvae appeared larger so we also used a non-subjective method of measuring terminal volume from 3D-rendered confocal images. Again, the type Ib terminals were significantly smaller than controls but, interestingly, the type Is terminals were unaffected (Fig. 2D). As a further measure of synapse size we counted the number of active zones at the NMJ. Active zones are visualized with an antibody to Bruchpilot (ELKS), an active zone component (Wagh et al., 2006). Bruchpilot positive puncta were counted at muscle 4 and this confirmed that the number of active zones within Ib boutons is reduced in *Cln7*$^{-/-}$ animals concomitant with the reduction in volume but is unchanged in type Is junctions (Fig. 2D). Both alleles of CLN7 had an identical phenotype as does the transheterozygous combination (Fig. 2E). Interestingly, both alleles were also haploinsufficient, suggesting some processes important for NMJ development are critically dependent on the levels of the CLN7 protein: potentially the stoichiometry of a membrane complex. These results suggest a requirement for Cln7 for normal development of the NMJ.

**Loss of Cln7 leads to synapse dysfunction**

To examine the consequence of the abnormal development of the synapse we characterized synaptic physiology and larval motility. An electrophysiological analysis of the NMJ was carried out using intracellular recordings. We recorded the spontaneous transmitter release at the larval NMJs for two minutes to calculate miniature excitatory

junction potential (mEJP) frequency and amplitude in 0.5, 0.75, 1.0 and 2.0 mM extracellular $Ca^{2+}$ concentration but there was no significant difference due to genotype in either case (Fig. 3A; 2-way ANOVA with Sidak's multiple comparison test, p=0.483). Taken together, we concluded there was likely to be little overt change in spontaneous synaptic vesicle release or post-synaptic receptor density.

Nerve-evoked excitatory junction potentials (EJPs), were recorded at 1Hz frequency at 1 mM extracellular $Ca^{2+}$ to evaluate synapse function. We found that EJPs at *Cln7* neuromuscular junctions were similar to those produced by control animals (Fig. 3C). We next applied continuous 5 Hz stimulation to the motor neurons to assess changes in the ability to recruit from the reserve pool of neurotransmitter vesicles. In the control animals, the evoked amplitudes followed a trend towards mild depression as vesicles in the reserve pool become depleted. However, a much more accentuated decline of EJP amplitude was observed in *Cln7* mutant animals under the same conditions (Fig. 3D). This suggests a potential defect in the ability of *Cln7* neurons to activate vesicles from the reserve pool or a defect in synaptic vesicle recycling.

The NMJs regulate body-wall muscle contraction. To identify if the electrophysiological changes we detected led to a quantifiable change in locomotion, we measured instantaneous speed of larval crawling. To address large variations in behavior within a population of larvae, and to avoid the tendency of larvae to avoid open fields, we used a custom 3D printed chamber to record the movement of multiple larvae simultaneously in oval "racetracks" over periods of 5 min (see methods). *Cln7* mutant larvae move significantly more slowly than isogenic control larvae (Fig. 3E).

**Cln7 function is required in the post-synaptic side of the NMJ**

Cln7 appears to be restricted to the post synaptic cell (Mohammed et al., 2017). To identify exactly which cells require Cln7 function at the synapse, we used standard GAL4 drivers to express dsRNA specifically targeted at CLN7 either pre-synaptically (Elav-Gal4), post-synaptically in the muscle (Mef2-Gal4), in all glia (Repo-Gal4) and in only the perineurial glia (PG-Gal4) that form the blood-brain-barrier, where Cln7 is highly expressed (Mohammed et al., 2017). Only knockdown of *Cln7* in the muscle replicated the under-development phenotype at the NMJ (Fig. 4A), consistent with very low or no expression of Cln7 in motoneurons. We performed the converse experiment of re-expressing YFP-Cln7 in

the *Cln7*$^{-/-}$ background, again with ubiquitous expression (actin-Gal4) or expression restricted to neurons (Elav-Gal4), to muscle (Mef2-Gal4), in both neurons and muscle together (Spin-Gal4) or to glia (Repo-Gal4). Only ubiquitous expression fully rescued the phenotype (Fig. 4B) indicating that some Cln7 function is required elsewhere in addition to the muscle.

**Autophagy is unaffected in Cln7 mutants**

Defects in the effectiveness of the autophagy pathway are associated with many forms of neurodegenerative disease, including forms of NCL (Seranova et al., 2017), and has been reported in a mouse model of CLN7 disease (Brandenstein et al., 2016). Impairment of autophagy is known to cause a reduction in synapse size similar to that seen in the *Cln7* mutants (Shen and Ganetzky, 2009). In cultured cells Cln7 is associated predominantly with lysosomes, which are essential mediators of autophagy and mutations affecting lysosomal function lead to a block in autophagic flux. Normal lysosomal function seems to be critical in the neuron (Milton et al., 2011; Sweeney and Davis, 2002; Wong et al., 2014; Wong et al., 2012), whereas Cln7 is restricted to the post-synaptic partner (Mohammed et al., 2017). . Therefore, we asked whether impaired autophagy in the *Cln7* flies might underpin the synaptic phenotypes.

We examined accumulation of p62, a multiple domain protein that acts as a receptor to activate autophagy. Under nutrient-rich conditions, p62 is usually degraded in lysosomes but in starvation conditions autophagic flux is increased and some non-degraded p62 accumulates in lysosomes (Fig. 5A, see $w^{1118}$ control). Thus, p62 levels are often monitored as one readout of autophagic flux. In *Cln7* larvae no p62 accumulates under growth conditions. However, a small but not statistically significant amount of p62 did accumulate under starvation conditions in the *Cln7* larvae, suggested a minor impairment in autophagy or lysosomal function (Fig. 6A and B). This contrasted markedly with *atg18* mutants. Here, p62 clearly accumulated during growth and did so very dramatically under starvation conditions (Fig. 5A and B).

We also examined whether increasing autophagic flux could rescue the *Cln7* phenotype by inhibiting the TOR complex activity using rapamycin or torin. TORC1 is a central regulator of growth and autophagy and homeostasis in cells and TORC2 is required

for normal NMJ development (Natarajan et al., 2013). Inhibition of TORC1 increases autophagic flux which, in the *Drosophila* NMJ, leads to an overgrowth phenotype (Shen and Ganetzky, 2009). Previously, it was reported that inhibiting TORC1 with rapamycin was unable to rescue the smaller NMJ phenotype seen in *atg18* mutants, presumably because autophagy is severely compromised in these animals and this cannot be circumvented (Shen and Ganetzky, 2009). We reasoned that rapamycin treatment would similarly have no effect on the *Cln7* phenotype if it was due to defective autophagy. However, both rapamycin treatment or treatment with the TORC1 and TORC2 inhibitor, torin, caused a very robust increase in NMJ size in both control and *Cln7* larvae indicating that autophagic flux can be increased (Fig. 5C). Taken together with the lack of p62 accumulation, this suggests that loss of Cln7 does not lead to an overt block in autophagy.

While autophagic flux is required to drive NMJ growth, TORC2 complex activity is necessary to restrict growth and loss of the TORC2-specific component, Rictor, leads to a large expansion of the NMJ (Natarajan et al., 2013). We wondered whether loss of Cln7 could affect TORC2 activity. We generated a $rictor^{\Delta 42}$;$Cln7^{84D}$ double mutant and saw a similar expansion of the synapse as in the *rictor* single mutant and consistent with the previous report (Fig. 5D; Natarajan et al., 2013). This places *Cln7* genetically upstream of TORC2 but, as with autophagic flux, TORC2 activity appears to be function principally in the neuron downstream of Tsc2 (Natarajan et al., 2013). Gven the restriction of Cln7 to the post-synaptic side, it is not likely to be directly acting on TORC2 in the neuron but could feasibly regulate a retrograde signal.

**Normal BMP retrograde signaling in Cln7 mutants**

Since Cln7 is required post-synaptically, we examined whether retrograde signaling necessary for normal growth of the pre-synaptic compartment of the NMJ might require Cln7 function. This retrograde signaling allows matching of pre-synapse size and excitability with muscle size. A key retrograde system is based on a BMP-type signal. Glass-bottomed boat (Gbb), a BMP molecule is secreted from the muscle and binds to Type I and II receptors Thick veins (Tkv), Saxophone (Sax) and Wishful thinking (Wit) expressed on the neuronal membrane. Ligand binding results in phosphorylation of the SMAD family member, Mothers against dpp (Mad) and its retrograde transport to the nucleus. Mutations in *gbb* or the receptors lead to loss of pMad and a smaller NMJ. Conversely, mutations in *Dad*, which

encodes an inhibitory SMAD, lead to NMJ synapse overgrowth and a profusion of small, satellite boutons (Aberle et al., 2002; McCabe et al., 2003; Rawson et al., 2003; Sweeney and Davis, 2002).

Given enrichment of Cln7 at the PSD and the similarity of the *Cln7* mutant phenotype to those seen for mutations in components of the BMP signaling pathway, we asked whether BMP retrograde signaling is affected by loss of *Cln7*. Potentially Cln7 might act in the post-synaptic muscle cell in the production, processing or presentation of the Gbb ligand. In this case, loss of *Cln7* would give an identical phenotype to loss of Gbb, Tkv, Sax or Wit but a double mutant combination would not make the synapse undergrowth phenotype worse. Similarly, loss of *Cln7* would abolish overgrowth in *Dad* mutants by preventing Mad phosphorylation downstream of Tkv and therefore *Dad;Cln7* double mutants should have a *Cln7*-like undergrowth. We quantified NMJ size in $sax^{4/5}$ and $Dad^{J1e4}$ single mutants and saw the expected undergrowth and overgrowth phenotypes respectively (Fig. 6A). The NMJ synapses size in *sax* mutants was almost identical to the $Cln7^{84D}$ mutants, however, a $sax^{4/5};Cln7^{84D}$ double mutant combination was lethal before late larval stage suggesting an additive effect and indicating that CLN7 and sax operate in different pathways. A $Dad^{J1e4};Cln7^{84D}$ double mutant combination showed a small reduction in overgrowth resulting in an intermediate phenotype. This suggests that phosphorylation of Mad in response to a Gbb signal is intact in the *Cln7* mutant larvae. To further confirm this, we stained the CNS of wild-type and *Cln7* larvae with anti-pMad. The nuclei of motor neurons clearly showed pMad present at the synapse in both genotypes (Fig. 6B).

**Cln7 as a negative regulator of TOR signaling**

As discussed above, TORC signaling regulates cell growth and autophagy. During our study, we noticed that the *Cln7* flies are considerably larger than their isogenic control lines (Fig. 7A). *Cln7* flies are not only heavier than controls, their body parts are also larger. We measured wing blade area from detached wings and identified a significant increase in *Cln7* animals *vs.* controls (Fig. 7B). Increased wing size could be due to additional cell divisions or due to cells growing larger. Additional divisions would suggest dysregulation of cell cycle controls but larger cells would indicate a potential hyper-activation of TORC. We counted the number of cells within 100µm$^2$ of the wing and found *Cln7* animals had fewer cells (125.7 cells [120.9-130.5 95% C.I.], n=10) than $w^{1118}$ control flies in the same area (138.1

cells [135-141.1], n=14; t-test p<0.0001). Thus, the cell size in *Cln7*$^{84D}$ flies is increased by 9.33% when compared to *w*$^{1118}$ control flies (p<0.0001, Fig. 7B). Initially, this suggested a dis-inhibition of TOR signaling in *Cln7* mutants.

**Deficiency in Cln7 is consistent with inhibition of TOR activity**

Potentially loss of Cln7 leads to an increase in TORC activity to generate larger flies. We attempted to block the overgrowth of Cln7 mutant flies during development by treatment with 1 μM rapamycin. Rapamycin is a potent inhibitor of TORC1 activity and chronic exposure is thought to also inhibit TORC2 (Sarbassov et al., 2006). Given the well-established role of TORC1 in promoting cellular growth, we were very surprised to see that administration of rapamycin to flies through their development from first instar larval stage actually leads to an *increase* in body mass in *w*$^{1118}$ control flies equal to that seen in *Cln7*$^{84D}$ flies (Fig. 7A). This surprising result argues instead that loss of *Cln7* leads to an *inhibition* of TORC activity. We looked for other phenotypes consistent with inhibition of TORC. In adult *Drosophila,* chronic rapamycin administration results in long-lived, stress resistance flies (Bjedov et al., 2010). We see similar phenotypes in *Cln7* adult flies (Fig. 7C and D).

Next, we looked for biochemical support that Cln7 helps regulate TORC activity. Rheb is a small GTPase located primarily in the lysosomal membrane and potentially co-located with Cln7, which also has a lysosomal location in cultured cells so we investigated whether Cln7 might be in a protein complex with Rheb. We expressed tagged forms of Cln7 and Rheb in *Drosophila* S2 cells and were able to co-immunoprecipitate the two proteins (Fig. 7E). Taken together, our data argue that Cln7 regulates TORC activity via Rheb postsynaptically to govern one aspect of retrograde signaling in the nervous system.

Finally, we sought to confirm a role for Cln7 in regulating TORC activity in mammalian cells. We nutrient-starved mouse embryonic fibroblasts from control and *Cln7* mutant mice (Brandenstein et al., 2016) then returned full-nutrient medium or medium lacking amino acids, glucose or insulin and looked for phosphorylation of p70 S6 kinase as a readout for TORC1 activity. We identified a clear requirement for Cln7 for full activation of TORC1 (Fig. 7F). This confirms and validates our findings in *Drosophila* and identifies a role for Cln7 in regulating TORC1 activity.

## Discussion

Here we have utilized *Drosophila* as a model system to identify an *in vivo* role for Cln7/MFSD8, the protein whose activity is reduced in late-infantile neuronal ceroid lipofuscinosis, an early onset childhood neurodegenerative disease. We demonstrate that Cln7 is required for normal synaptic development consistent with a growing appreciation that the synapse is a significant target in neurodegenerative disease. When Cln7 is disrupted, the *Drosophila* neuromuscular junction fails to reach its normal size having a reduced volume while maintaining normal active zone density. While this is characteristic of mutations affecting autophagic flux within neurons, autophagy is only mildly affected by loss of Cln7. Instead, Cln7 appears to function on the post-synaptic side of the junction and be required for full activation of TOR signaling. Previous studies have revealed that TOR signaling has a conserved postsynaptic role to influence retrograde regulation of synaptic activity at central and peripheral synapses in both *Drosophila* and vertebrates (Henry et al., 2018; Penney et al., 2012) and that dysregulation of TORC signaling is associated with autism and cognitive decline (Lipton and Sahin, 2014). We demonstrate that late-infantile NCL may additionally be a consequence of an early failure of synapse development brought about by inappropriate regulation of TORC signaling.

### Lysosome protein function in neural development

Neuronal ceroid lipofuscinosis is a disease with multiple forms with varied ages of onset; lysosomal dysfunction is a common feature. Lysosomal function is essential for autophagic flux and autophagic dysfunction is reported in a Cln7 mutant mouse model, consistent with a predominantly lysosomal localization for the Cln7 protein (Brandenstein et al., 2016). Autopahgy is also essential for neural development and long-term neural health, including in *Drosophila.* Given the similarity of the NMJ phenotype in *Cln7* and various *atg* mutants (Shen and Ganetzky, 2009), we assumed defective autophagy was likely responsible for the *Cln7* phenotypes. However, autophagy appears to be required in the neuron rather than post-synaptically and, while we cannot rule out a small contribution, we demonstrate here that autophagy is largely intact in the absence of Cln7.

Mutations in other lysosomal genes also affect NMJ development but these appear to act predominantly pre-synaptically in the neuron. Two notable examples are Spinster –

like Cln7 an MFS-domain protein – which localize to late endosomes and lysosomes in both neurons and muscle; and Trpml, a lysosomal cation channel and homologue of the gene mutated in the human lysosomal storage disorder, mucolipodosis type IV. In Spinster mutants, a large overgrowth of the NMJ occurs due to excess reactive oxygen species being generated in the neurons (ROS are a cell-autonomous driver of neural growth in this system; (Milton et al., 2011)). The retrograde BMP signaling that drives pre-synaptic expansion is also potentiated in the Spinster mutants, presumably due to inefficient degradation of the active ligand/receptor complex (Sweeney and Davis, 2002). In Trpml mutants, a similar undergrowth of the NMJ occurs to that in Cln7 mutants (Wong et al., 2014). Trpml functions as a $Ca^{2+}$ channel in lysosomes and by regulating an important aspect of lysosomal function –storage of intracellular $Ca^{2+}$ – also regulates autophagy and TORC1 activity (Wong et al., 2012). However, like Spinster and in contrast to Cln7, Trmpl is required pre-synaptically. Here we demonstrate a post-synaptic specificity for Cln7 that exposes a potential new mechanism for regulating neural development and function.

Cln7 regulates TORC function

Our unexpected finding that rapamycin treatment throughout larval development leads to increased organismal growth seems counterintuitive, given the well-understood role of TORC1 in promoting growth. To the best of our knowledge, this result has not been reported before and it is not clear what compensatory pathways might be being activated by this chronic inhibition of TORC activity throughout development. Nor can we can find reports of the effects of rapamycin administration throughout embryonic development on the growth of mammals from which we might draw comparisons. Further studies will be needed to identify the downstream effects of rapamycin during development.

TORC1 and TORC2 activity in neural development

The mTORC1 complex has a well-established role regulating neural growth and development in the mammalian nervous system. Several activating mutations upstream of mTORC1, including loss of PTEN or Tsc1/2, result in overgrowth of neurons and increase in density of dendritic spines, as do mutations in the translational repressor, FRMP, downstream of active mTORC1. Consistent with these effects, autism is a highly prevalent co-morbid feature in human disorders caused by mutations in these genes, including tuberous sclerosis,

PTEN harmatoma syndrome and Fragile-X syndrome (Lipton and Sahin, 2014). TORC1 activity also has conserved function regulating synaptic homeostasis (Henry et al., 2018; Penney et al., 2012).

Much less is understood about the role of the mTORC2 complex in the CNS although deletion of the TORC2-specific component, rictor, in all neurons or specifically in Purkinje cells causes deficits in neural growth and development, including morphological effects with consequential early-onset motor deficits which are reminiscent of the *Drosophila* effects described here (Angliker et al., 2015; Thomanetz et al., 2013). However, the reports of TORC2 requirement at the *Drosophila* NMJ are not consistent: Natarajan and colleagues (Natarajan et al., 2013) show a large increase in NMJ size in rictor mutants (and we confirm this effect in our study). In this scenario, Tsc2 negatively regulates Rheb upstream of TORC2 in the neuron and argues that TORC2 activity restricts neural growth. In contrast, Dimitroff et al, (Dimitroff et al., 2012) suggest the opposite: that TORC2 activity is required for expansion. The paradox may simply be due to different rictor alleles used, however, the Purkinje cells lacking rictor are smaller than controls (Thomanetz et al., 2013). Our identification of a protein complex containing Cln7 and Rheb places Cln7 in the regulation framework governing TORC activity in neurons but exactly how it functions will require identification of the other proteins in the complex and an understanding of the cargo transported by the Cln7 protein.

Implications for the NCLs

Changes in synapse function have been seen in various models of CLN1 and CLN3 disease and may well be universal to the NCLs e.g. (Aby et al., 2013; Grunewald et al., 2017; Kim et al., 2008; Llavero Hurtado et al., 2017). CNS pathology manifests very early in life in CLN7 disease so it is possible that developmental changes to the CNS and synaptic abnormalities – if also present in human CLN7 disease – predicate for later neuropathology, although potential mechanisms driving this are not yet clear. Might the failure to activate TORC activity underpin degeneration? The effects of over-activation of mTORC1 through loss of inhibitory factors, Tsc1/2 or PTEN, or overexpression of the activator, Rheb, are well understood and can include neurodevelopmental disorders, epilepsy and neuroblastoma (Lipton and Sahin, 2014). Similarly, a role for TORC signaling in synaptic homeostasis have been reported in various systems (Bateup et al., 2013; Henry et al., 2018; Penney et al., 2012). It will be of interest to identify if TORC-dependent processes are affected in the CNS

of the Cln7 deficient mouse model. Lysosomal $Ca^{2+}$ homeostasis is affected in several lysosomal disorders, including CLN3 disease (Chandrachud et al., 2015) and, while Cln7 is not likely to be a $Ca^{2+}$ channel, it will be interesting to ask if changes to $Ca^{2+}$ accompany and potentially underpin the loss of post-synaptic TORC activity in Cln7 mutants, as they appear to pre-synaptically in Trmpl mutants (Wong et al., 2012). Many of the CLN proteins are considered to be lysosomal but lysosomes are predominantly localized in a peri-nuclear location in neurons. The emerging story of synaptic dysfunction in the NCLs either reflects alternative localization *in vivo* in the CNS or remote influence of lysosomes on synaptic function (or both). Here, Cln7 is post-synaptic and enriched at the PSD so it will be interesting to identify if this is true also for the Cln7 protein in the mammalian CNS *in vivo.*

## Materials and Methods

### *Drosophila* husbandry.

Flies were maintained at 25 °C, 65% humidity on a 12 h light:dark cycle on standard agar-based food. "German food" (0.8% w/v agar, 8% w/v yeast, 2% w/v yeast extract, 2% w/v peptone, 3% w/v sucrose, 6% w/v glucose, 0.05% magnesium sulphate and 0.05% calcium chloride) was used on occasions to boost egg laying when building strains and for NMJ quantification and larval movement assays. Both food recipes were supplemented with p-Hydroxy-benzoic acid methyl ester at 0.1% final concentration from a 10% w/v solution in ethanol and 0.3% v/v propionic acid as antifungal agents. For adult mass assay, SY food was used without anti-fungals (Chapman and Partridge, 1996). For 1$^{st}$ instar larval collection, adult flies were mated in 90 mm diameter cages and females allowed to lay eggs for 20-24 h on 10% v/v grape juice, 2.5% agar petri plates seeded with fresh baker's yeast. After changing, plates were returned to the incubator for 24 h to allow embryos to hatch into larvae.

### *Drosophila* lines.

Flies lines were obtained from the Bloomington Stock Center at Indiana University except for an isogenic $w^{1118}$ control strain from the Vienna *Drosophila* Resource Center; PG-Gal4 (NP6293) from the Kyoto DGRC Stock Center; Spin-Gal4 and $Dad^{j1e4}$ from Dr. Sean Sweeney (University of York, UK); and $rictor^{\Delta 42}$ from Dr. Joseph Bateman (King's College London). Gal4 lines used with stock numbers as of March 2018 were as follows: actin (BL3954); Elav c155 (BL458); Mef2 (BL27930); vGlut (BL26160); Repo (7415); PG (Kyoto: 105188). The Cln7 RNAi line used was yv;TRiP.HMC03819 (BL55664). Standard mating schemes and balancer chromosomes were used to generate genetic combinations and recombinations as appropriate.

The Venus-YFP-Cln7 knock-in reporter was generated in the Tuxworth lab previously by CRISPR/Cas9-mediated gene editing (Mohammed et al., 2017). To generate UAS-Venus-Cln7, the full-length Cln7 ORF was amplified by proofreading PCR using clone GH22722 as a template and cloned into pENTR (Thermo). After sequence verification it was recombined into the pTVW destination vector obtained from the *Drosophila* Genetics Resource Center, University of Indiana and injected by BestGene Inc. to generate transformants. Insertions were mapped to chromosomes by standard mating schemes.

### Generation of Cln7 mutants.

The P-element NP0345 inserted in the 5'UTR of the *Cln7* locus (CG8596) was excised by mating with to the $\Delta$2-3 transposase line. Germline excision events were isolated with a standard crossing scheme and deletion events detected by PCR from gDNA. Two independent alleles, 36H and 84D, in which

the loci either side of CG8596 were intact, were selected for study. Both alleles were backcrossed over 6 generations to the isogenic $w^{1118}$ control.

**Adult mass assays**

Cohorts of 100 first instar larvae were transferred from grape juice agar plates to vials of SY food and allowed to develop until eclosion. Flies were weighed in Eppendorf tubes in groups of 20. Rapamycin was added to molten SY food at 50 °C to 1 μM final concentration from a stock solution of 20 mM in ethanol.

**Lifespan and stress assays**

Homozygous $Cln7^{84D}$, $Cln3^{\Delta MB1}$ (Tuxworth et al., 2011) and isogenic $w^{1118}$ control flies were reared in uncrowded conditions in bottles on standard food and allowed to mate for 2 days after eclosion. On day 3, 100 females of each genotype were separated into 5 vials of 20 flies each. For lifespan, death was recorded every 2 days. For paraquat assays, vials contained 1% LMP agarose, 10 mM methyl viologen (MP Biomedicals) in water and deaths were recorded 2-3 times per day. Survival data was plotted in Prism 7 and analyzed by Log-Rank test.

**Visualization of the larval NMJ and CNS**

Alexa-594 goat anti-HRP was used to visualize the pre-synaptic membrane except for volume measurements from confocal z-sections when a membrane-localized GFP was used. For this, the glutamatergic vGlut-Gal4 driver (OK371-Gal4) was recombined with UAS-CD8::GFP on chromosome 2 then combined with the wild-type, $Cln7^{36H}$ or $Cln7^{84D}$ alleles on chromosome 3. All strains were outcrossed to an isogenic $w^{1118}$ beforehand over six generations. To ensure constant culture density and conditions between samples, cohorts of 100 1$^{st}$ instar larvae were picked from the agar plates and transferred to vials of freshly made German food and incubated for 3-4 days until wandering 3$^{rd}$ instar stage. Larvae were dissected in HL3.1 containing 1 mM EDTA according to (Mohammed et al., 2017). Following dissection, larvae were fixed in 4% EM-grade formaldehyde (Polysciences) diluted in HL3.1 for 20 min then washed and permeabilized in PBS, 0.1 % Triton X-100 (PBST) and blocked in 1% BSA in PBST for 30-60 min. Preps were incubated in primary antibodies in block overnight at 4 °C and in secondary antibodies for 2-4 h at RT. Washing steps after each antibody were with multiple changes of PBST for approximately 1 h at RT. Finally, preps were mounted in Prolong Gold (Thermo) and visualized on a Zeiss LSM510 Meta or LSM780 confocal microscope.

**Antibodies for immunofluorescence**

Pre-synaptic membrane was visualized with goat anti-HRP directly conjugated to Alexa-594 (1:1000; Jackson Immuno) or rabbit anti-GFP (1:1000, AbCam). Active zones were stained with mouse anti-Bruchpilot (clone NC82, 1:25; Developmental Studies Hybridoma Bank) and post-synaptic densities with anti-Dlg (clone 4F3, 1:20; DSHB). Rabbit anti-pMAD (1:500) was a gift of Prof. Carl-Henrik Heldin (Ludwig Institute for Cancer Research, Uppsala). Venus-YFP-Cln7 was visualized with rabbit anti-GFP. Secondary antibodies were labeled with Alexa-488, Alexa-543, Alexa-596 or Alexa-633 (Thermo or Jackson Immuno, all 1:500).

**Quantification of NMJ size**

For measurement of pre-synaptic size from confocal images, volumes were acquired from type Ib and Is junctions innervating muscle 4 of segments A3-5 from vGlut-Gal4, UAS-CD8::GFP-expressing larvae stained with anti-GFP and anti-Bruchpilot as above. Volumes were acquired with an optical width of 1.0 μM and steps of 0.5 μM using a 40x N.A. 1.4 PlanApo objective and zoom = 2.0. Volocity (Perkin Elmer) was used to render the volumes then built in quantification routines used to measure the volume of the pre-synaptic membrane and to count active zones.

For manual bouton counts, larvae were stained with Alexa-594-conjugated goat anti-HRP then visualized on an upright Zeiss AxioPlan2 compound microscope using a Plan NeuoFluor 40X 0.75 N.A. air immersion objective. Boutons were scored as swellings in the type Ib junction on muscle 4 of segments A3-A5. In each case a transmitted light image of the corresponding muscle was obtained at 10x using an AxioCam and the muscle surface area calculated by outlining in ImageJ. Bouton number was then normalized to the muscle surface area.

**Quantification of larval movement**

Cohorts of 1$^{st}$ instar larvae were transferred to German food vials as above. At wandering 3$^{rd}$ instar stage they were removed from the wall of the vial, transferred to a small petri plate containing Sylgard and then to the troughs of a custom 3D-printed translucent chamber. The chamber comprises 12 oval troughs approximately 3 mm deep and with a track length of 75 mm. Since the larvae do not move well on the plastic, each trough was lined with a thin coating of 3% w/v agar. The chamber was lit from below by a LED light table and filmed from above with a Basler GigE camera. Cohorts of 12 larvae crawling were filmed for 5 min each and their position tracked at 2.5 fps using Ethovision software (Noldus). Larvae crawl around the trough but rarely climb out: any that did were discounted from the analysis. Instantaneous speed data was exported from Ethovision and analyzed in Prism 7.0 (Graphpad).

**Electrophysiology**

Wandering 3rd instar larvae were dissected in HL3.1 supplemented with $Ca^{2+}$ concentration at 0.5, 0.75, 1.0 or 2.0 mM depending on the paradigm (Stewart et al., 1994). Recordings were made from muscle 4 of segments A3-A5 using standard protocols (Zhang and Stewart, 2010). Baseline synaptic transmission was characterized by recording mEJPs for 2 min and 16 EJPs stimulated at 1 Hz. For high frequency stimulation, 16 EPSPs at 1 Hz were recorded followed by 5 Hz stimulation for 5 min. In all experiments a minimum of 8 larvae were used with maximum of 2 recordings per larva. In each case the starting resting potential of the muscle was -60 to -75 mV and resistance of 5-10 mΩ. Analysis of electrophysiological recordings was performed in Clampfit 10.0 (Molecular Devices) and data exported for further analysis in Prism 7.0 (Graphpad).

***Drosophila* starvation assay**

First instar larvae of control $w^{1118}$, $Cln7^{84D}$ and Atg18a$^{KG03090/}$Df(3L)Exel6112 were transferred in cohorts of 20 from grape juice agar plates to standard food vials smeared with fresh yeast paste and allowed to develop for a further 24 h at 25 °C. Larvae were then removed from the food and protein samples prepared for each genotype. The remaining 10 larvae for each genotype were starved of amino acids for 4 h at 25 °C by washing them twice in PBS spray before transferring to vials containing 20% w/v sucrose. Lysates of total protein were prepared by manually crushing the larvae with a mini-pestle directly into 200 μl Laemlli buffer containing 8 mM DTT and protease inhibitors. TMB6B, Tb balancer chromosomes were used to identify the Atg18a/Df genotype.

**Cell starvation assay**

Mouse embryonic fibroblasts derived from control and $Mfsd8^{(tm1d/tm1d)}$ mice (Brandenstein et al., 2016) were a kind gift of Dr. Stephan Storch, University Medical Centre Hamburg-Eppendorf. Cells were cultured in DMEM + 10% FCS (both Gibco) at 37 °C, 5% $CO_2$. For starvation, cells were seeded at 0.75 x $10^6$ cells/ml in 6-well plates and grown overnight. Next day, cells were washed twice then incubated for 24 h in EBBS (Gibco) at 37 °C, 5% $CO_2$. For full nutrient replacement, EBBS was replaced by EBBS supplemented with 10 % dialysed serum (US Biologicals); 1 x amino acid supplement (Gibco); 5.5 mM D-glucose and 4 μg/ml insulin (Gibco). To test requirements for each component, replacement medium was used lacking amino acids or glucose or both serum and insulin but containing each of the other components at the same concentrations. 1 h after nutrient replacement cells were lysed in RIPA buffer then clarified by centrifugation at 15,000 x g for 10 min at 4 °C. Laemlli buffer was added then samples heated to 70 °C for 5 min before loading on protein gels.

**Cell transfection and immunoprecipitation.**

To generate expression plasmids, the Cln7 pENTR clone was recombined into pAMW. The full-length Rheb ORF was amplified from clone GH10361 and cloned in to pENTR. After sequence verification it was recombined in pAFW.

*Drosophila* S2 cells were seeded in 6-well plates at $3x10^6$ cells/well in 2 ml Schneider's + 10% FCS and settled for 24 h prior to transfection. A total of 2.5 µg DNA was transfected per well at a ratio of 1 µg DNA:3 µl TransIT-2020 transfection reagent (MirusBio). Cells were harvested 24 h post-transfection, washed once in PBS then lysed in 0.5 ml lysis buffer (25 mM Tris.HCl, pH 7.5; 150 mM NaCl; 5 mM $MgCl_2$; 1 mM Na.EDTA, pH 8.0; 2% w/v dodecyl maltoside; 1:200 protease inhibitors (Calbiochem). Tagged proteins were immunoprecipitated with Myc-Trap_MA beads (ChromoTek) or anti-FLAG M2 Affinity gel (Sigma) overnight at 4°C. Beads were washed five times in wash buffer (identical to lysis buffer except 0.5% w/v dodecyl maltoside) then eluted in 50 µl 0.2 M glycine.HCl, pH 2.5 and neutralized with 5 µl 1M Tris.HCl, pH 10. Samples for Western blot were prepared in 1X Laemlli buffer and heated at 70°C for 5 min prior to loading onto gels.

**Western blotting**

Protein were separated by standard SDS-PAGE and transferred to PVDF membranes by wet transfer. Membranes were blocked in 5% milk in TBS + 0.1% Tween-20 (TBST) for 30 min then incubated in primary antibodies in milk/TBST overnight at 4 °C and secondary antibodies for 1 h at RT. Washing after each antibody was with 5-6 x 5 min in TBST. Primary antibodies were: mouse anti-Flag M2 (1:5000; Sigma); goat anti-myc (1:1000; AbCam); rabbit anti-Ref(2)P (*Drosophila* homologue of p62, 1:500; a gift of Dr. Gabor Juhasz, Eötvös Loránd University, Budapest); rabbit anti-p70 S6K pThr389 (1:500; Cell Signaling Technologies) and mouse anti-actin (clone JLA-20, 1:500; DSHB). Secondary antibodies were HRP-conjugated goat anti-mouse or anti-rabbit IgG (both 1:4000, Cell Signaling Technologies). Detection of HRP was with SuperSignal West pico ECL reagent (Pierce) in conjunction with a Vilber Fusion FX system. p62 levels were normalized to actin from 16-bit images using ImageJ.

**Statistical analysis**

All statistical tests were performed within Prism 7 (Graphpad). Normality of datasets was determined using a D'Agostino-Pearson test and datasets not conforming to Gaussian distributions were transformed with logarithmic or reciprocal transformations. Non-parametric tests were used where distributions remained non-Gaussian after transformation. Samples sizes and tests used are described in the figure legends. Significance in all cases was set at $p<0.05$.

**Acknowledgements**

The authors are very grateful to Dr. Stephan Storch for sharing the *Cln7*$^{tm1d/tm1d}$ mouse embryonic fibroblasts ahead of publication; to Drs. Sean Sweeney and Joe Bateman for sending *Drosophila* lines; to Dr. Gabor Juhasz and Prof. Carl-Henrik Heldin for the anti-Ref(2)P and pMad antibodies respectively; and would like to thank Dr. Cathy Slack for her help comments on the manuscript. Research was funded by The Wellcome Trust grant number 082004 to GT and by a UK Biotechnology and Biological Sciences Research Council New Investigator award BB/N008472/1 to RIT. BAS was supported by a Natural Sciences and Engineering Research Council of Canada grant number 250078. MBO was supported by a King's College, London Quota BBSRC PhD studentship and a KCL Peter Baker Travelling Fellowship. AM and KJC were supported by University of Birmingham College of Medical and Dental Sciences PhD studentship awards. The authors declare no competing financial interests.

**Author contributions**

Megan O'Hare generated the *Cln7* mutations; MO'H, Alamin Mohammed, Katelyn Aitchison, Niki Anthoney and Richard Tuxworth generated synapse data; Kyle Connolly generated fly mass data and co-IP results; AM generated the *Drosophila* starvation data and KC and Amy Roberts the MEF cell starvation data; KMA and RIT performed speed analysis; MBO and BAS generated electrophysiology data. All authors contributed to data analysis and figure preparation. RIT and GT raised funding for the project and wrote the manuscript.

## References


Aberle, H., A.P. Haghighi, R.D. Fetter, B.D. McCabe, T.R. Magalhaes, and C.S. Goodman. 2002. wishful thinking encodes a BMP type II receptor that regulates synaptic growth in Drosophila. *Neuron*. 33:545-58.

Aby, E., K. Gumps, A. Roth, S. Sigmon, S.E. Jenkins, J.J. Kim, N.J. Kramer, K.D. Parfitt, and C.A. Korey. 2013. Mutations in palmitoyl-protein thioesterase 1 alter exocytosis and endocytosis at synapses in Drosophila larvae. *Fly (Austin)*. 7:267-79.

Angliker, N., M. Burri, M. Zaichuk, J.M. Fritschy, and M.A. Ruegg. 2015. mTORC1 and mTORC2 have largely distinct functions in Purkinje cells. *Eur J Neurosci*. 42:2595-612.

Bateup, H.S., C.A. Johnson, C.L. Denefrio, J.L. Saulnier, K. Kornacker, and B.L. Sabatini. 2013. Excitatory/inhibitory synaptic imbalance leads to hippocampal hyperexcitability in mouse models of tuberous sclerosis. *Neuron*. 78:510-22.

Bjedov, I., J.M. Toivonen, F. Kerr, C. Slack, J. Jacobson, A. Foley, and L. Partridge. 2010. Mechanisms of life span extension by rapamycin in the fruit fly Drosophila melanogaster. *Cell Metab*. 11:35-46.

Brandenstein, L., M. Schweizer, J. Sedlacik, J. Fiehler, and S. Storch. 2016. Lysosomal dysfunction and impaired autophagy in a novel mouse model deficient for the lysosomal membrane protein Cln7. *Hum Mol Genet*. 25:777-91.

Chandrachud, U., M.W. Walker, A.M. Simas, S. Heetveld, A. Petcherski, M. Klein, H. Oh, P. Wolf, W.N. Zhao, S. Norton, S.J. Haggarty, E. Lloyd-Evans, and S.L. Cotman. 2015. Unbiased Cell-based Screening in a Neuronal Cell Model of Batten Disease Highlights an Interaction between Ca2+ Homeostasis, Autophagy, and CLN3 Protein Function. *J Biol Chem*. 290:14361-80.

Chapel, A., S. Kieffer-Jaquinod, C. Sagne, Q. Verdon, C. Ivaldi, M. Mellal, J. Thirion, M. Jadot, C. Bruley, J. Garin, B. Gasnier, and A. Journet. 2013. An extended proteome map of the lysosomal membrane reveals novel potential transporters. *Mol Cell Proteomics*. 12:1572-88.

Chapman, T., and L. Partridge. 1996. Female fitness in Drosophila melanogaster: an interaction between the effect of nutrition and of encounter rate with males. *Proc Biol Sci*. 263:755-9.

Charng, W.L., S. Yamamoto, and H.J. Bellen. 2014. Shared mechanisms between Drosophila peripheral nervous system development and human neurodegenerative diseases. *Curr Opin Neurobiol*. 27:158-64.

Dimitroff, B., K. Howe, A. Watson, B. Campion, H.G. Lee, N. Zhao, M.B. O'Connor, T.P. Neufeld, and S.B. Selleck. 2012. Diet and energy-sensing inputs affect TorC1-mediated axon misrouting but not TorC2-directed synapse growth in a Drosophila model of tuberous sclerosis. *PLoS One*. 7:e30722.

Frank, C.A. 2014. Homeostatic plasticity at the Drosophila neuromuscular junction. *Neuropharmacology*. 78:63-74.

Grunewald, B., M.D. Lange, C. Werner, A. O'Leary, A. Weishaupt, S. Popp, D.A. Pearce, H. Wiendl, A. Reif, H.C. Pape, K.V. Toyka, C. Sommer, and C. Geis. 2017. Defective synaptic transmission causes disease signs in a mouse model of juvenile neuronal ceroid lipofuscinosis. *Elife*. 6.

Henry, F.E., X. Wang, D. Serrano, A.S. Perez, C.J.L. Carruthers, E.L. Stuenkel, and M.A. Sutton. 2018. A Unique Homeostatic Signaling Pathway Links Synaptic Inactivity to Postsynaptic mTORC1. *J Neurosci*. 38:2207-2225.

Jalanko, A., and T. Braulke. 2009. Neuronal ceroid lipofuscinoses. *Biochim Biophys Acta*. 1793:697-709.

Kielar, C., T.M. Wishart, A. Palmer, S. Dihanich, A.M. Wong, S.L. Macauley, C.H. Chan, M.S. Sands, D.A. Pearce, J.D. Cooper, and T.H. Gillingwater. 2009. Molecular correlates of axonal and synaptic pathology in mouse models of Batten disease. *Hum Mol Genet*. 18:4066-80.

Kim, S.J., Z. Zhang, C. Sarkar, P.C. Tsai, Y.C. Lee, L. Dye, and A.B. Mukherjee. 2008. Palmitoyl protein thioesterase-1 deficiency impairs synaptic vesicle recycling at nerve terminals, contributing to neuropathology in humans and mice. *J Clin Invest*. 118:3075-86.

Koch, S., S.M. Molchanova, A.K. Wright, A. Edwards, J.D. Cooper, T. Taira, T.H. Gillingwater, and J. Tyynela. 2011. Morphologic and functional correlates of synaptic pathology in the cathepsin D knockout mouse model of congenital neuronal ceroid lipofuscinosis. *J Neuropathol Exp Neurol*. 70:1089-96.

Kousi, M., E. Siintola, L. Dvorakova, H. Vlaskova, J. Turnbull, M. Topcu, D. Yuksel, S. Gokben, B.A. Minassian, M. Elleder, S.E. Mole, and A.E. Lehesjoki. 2009. Mutations in CLN7/MFSD8 are a common cause of variant late-infantile neuronal ceroid lipofuscinosis. *Brain*. 132:810-9.

Lipton, J.O., and M. Sahin. 2014. The neurology of mTOR. *Neuron*. 84:275-91.

Llavero Hurtado, M., H.R. Fuller, A.M.S. Wong, S.L. Eaton, T.H. Gillingwater, G. Pennetta, J.D. Cooper, and T.M. Wishart. 2017. Proteomic mapping of differentially vulnerable pre-synaptic populations identifies regulators of neuronal stability in vivo. *Sci Rep*. 7:12412.

Lnenicka, G.A., and H. Keshishian. 2000. Identified motor terminals in Drosophila larvae show distinct differences in morphology and physiology. *J Neurobiol*. 43:186-97.

McCabe, B.D., G. Marques, A.P. Haghighi, R.D. Fetter, M.L. Crotty, T.E. Haerry, C.S. Goodman, and M.B. O'Connor. 2003. The BMP homolog Gbb provides a retrograde signal that regulates synaptic growth at the Drosophila neuromuscular junction. *Neuron*. 39:241-54.

Milton, V.J., H.E. Jarrett, K. Gowers, S. Chalak, L. Briggs, I.M. Robinson, and S.T. Sweeney. 2011. Oxidative stress induces overgrowth of the Drosophila neuromuscular junction. *Proc Natl Acad Sci U S A*. 108:17521-6.

Mohammed, A., M.B. O'Hare, A. Warley, G. Tear, and R.I. Tuxworth. 2017. in vivo localization of the neuronal ceroid lipofuscinosis proteins, CLN3 and CLN7, at endogenous expression levels. *Neurobiol Dis*. 103:123-132.

Muzaffar, N.E., and D.A. Pearce. 2008. Analysis of NCL Proteins from an Evolutionary Standpoint. *Curr Genomics*. 9:115-36.

Natarajan, R., D. Trivedi-Vyas, and Y.P. Wairkar. 2013. Tuberous sclerosis complex regulates Drosophila neuromuscular junction growth via the TORC2/Akt pathway. *Hum Mol Genet*. 22:2010-23.

Penney, J., K. Tsurudome, E.H. Liao, F. Elazzouzi, M. Livingstone, M. Gonzalez, N. Sonenberg, and A.P. Haghighi. 2012. TOR is required for the retrograde regulation of synaptic homeostasis at the Drosophila neuromuscular junction. *Neuron*. 74:166-78.

Rawson, J.M., M. Lee, E.L. Kennedy, and S.B. Selleck. 2003. Drosophila neuromuscular synapse assembly and function require the TGF-beta type I receptor saxophone and the transcription factor Mad. *J Neurobiol*. 55:134-50.

Sarbassov, D.D., S.M. Ali, S. Sengupta, J.H. Sheen, P.P. Hsu, A.F. Bagley, A.L. Markhard, and D.M. Sabatini. 2006. Prolonged rapamycin treatment inhibits mTORC2 assembly and Akt/PKB. *Mol Cell*. 22:159-68.

Seranova, E., K.J. Connolly, M. Zatyka, T.R. Rosenstock, T. Barrett, R.I. Tuxworth, and S. Sarkar. 2017. Dysregulation of autophagy as a common mechanism in lysosomal storage diseases. *Essays Biochem*. 61:733-749.

Sharifi, A., M. Kousi, C. Sagne, G.C. Bellenchi, L. Morel, M. Darmon, H. Hulkova, R. Ruivo, C. Debacker, S. El Mestikawy, M. Elleder, A.E. Lehesjoki, A. Jalanko, B. Gasnier, and A. Kyttala. 2010. Expression and lysosomal targeting of CLN7, a major facilitator superfamily transporter associated with variant late-infantile neuronal ceroid lipofuscinosis. *Hum Mol Genet*. 19:4497-514.

Shen, W., and B. Ganetzky. 2009. Autophagy promotes synapse development in Drosophila. *J Cell Biol*. 187:71-9.

Siintola, E., M. Topcu, N. Aula, H. Lohi, B.A. Minassian, A.D. Paterson, X.Q. Liu, C. Wilson, U. Lahtinen, A.K. Anttonen, and A.E. Lehesjoki. 2007. The novel neuronal ceroid lipofuscinosis gene MFSD8 encodes a putative lysosomal transporter. *Am J Hum Genet*. 81:136-46.

Steenhuis, P., S. Herder, S. Gelis, T. Braulke, and S. Storch. 2010. Lysosomal targeting of the CLN7 membrane glycoprotein and transport via the plasma membrane require a dileucine motif. *Traffic*. 11:987-1000.

Stewart, B.A., H.L. Atwood, J.J. Renger, J. Wang, and C.F. Wu. 1994. Improved stability of Drosophila larval neuromuscular preparations in haemolymph-like physiological solutions. *J Comp Physiol A*. 175:179-91.

Sweeney, S.T., and G.W. Davis. 2002. Unrestricted synaptic growth in spinster-a late endosomal protein implicated in TGF-beta-mediated synaptic growth regulation. *Neuron*. 36:403-16.

Thomanetz, V., N. Angliker, D. Cloetta, R.M. Lustenberger, M. Schweighauser, F. Oliveri, N. Suzuki, and M.A. Ruegg. 2013. Ablation of the mTORC2 component rictor in brain or Purkinje cells affects size and neuron morphology. *J Cell Biol*. 201:293-308.

Tuxworth, R.I., H. Chen, V. Vivancos, N. Carvajal, X. Huang, and G. Tear. 2011. The Batten disease gene CLN3 is required for the response to oxidative stress. *Hum Mol Genet*. 20:2037-47.

Wagh, D.A., T.M. Rasse, E. Asan, A. Hofbauer, I. Schwenkert, H. Durrbeck, S. Buchner, M.C. Dabauvalle, M. Schmidt, G. Qin, C. Wichmann, R. Kittel, S.J. Sigrist, and E. Buchner. 2006. Bruchpilot, a protein with homology to ELKS/CAST, is required for structural integrity and function of synaptic active zones in Drosophila. *Neuron*. 49:833-44.

Wong, C.O., K. Chen, Y.Q. Lin, Y. Chao, L. Duraine, Z. Lu, W.H. Yoon, J.M. Sullivan, G.T. Broadhead, C.J. Sumner, T.E. Lloyd, G.T. Macleod, H.J. Bellen, and K. Venkatachalam. 2014. A TRPV channel in Drosophila motor neurons regulates presynaptic resting Ca2+ levels, synapse growth, and synaptic transmission. *Neuron*. 84:764-77.

Wong, C.O., R. Li, C. Montell, and K. Venkatachalam. 2012. Drosophila TRPML is required for TORC1 activation. *Curr Biol*. 22:1616-21.

Zhang, B., and B. Stewart. 2010. Electrophysiological recording from Drosophila larval body-wall muscles. *Cold Spring Harb Protoc*. 2010:pdb prot5487.

# Figure 1

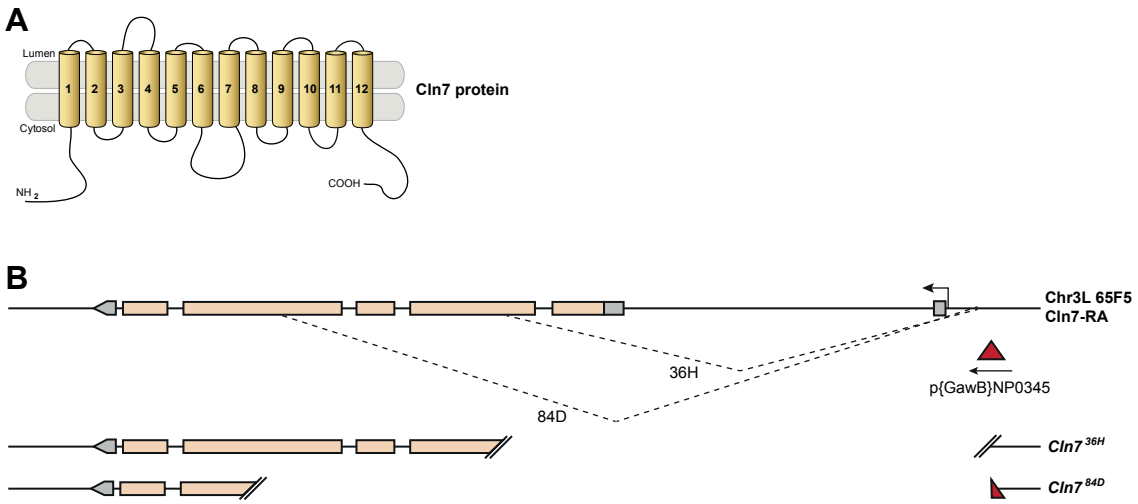


*Figure 1. Generation of Cln7 mutations*

*A. Cln7 is predicted to be a 12-span transmembrane protein and member of the multifacilitator superfamily of solute transporters.*
*B. P-element-mediated imprecise excision was used to generate deletions within the Cln7 locus (CG8596). Two unidirectional deletion events, 36H and 84D, are shown diagrammatically. Some of the P-element sequence is retained in the 84D allele.*

Figure 2

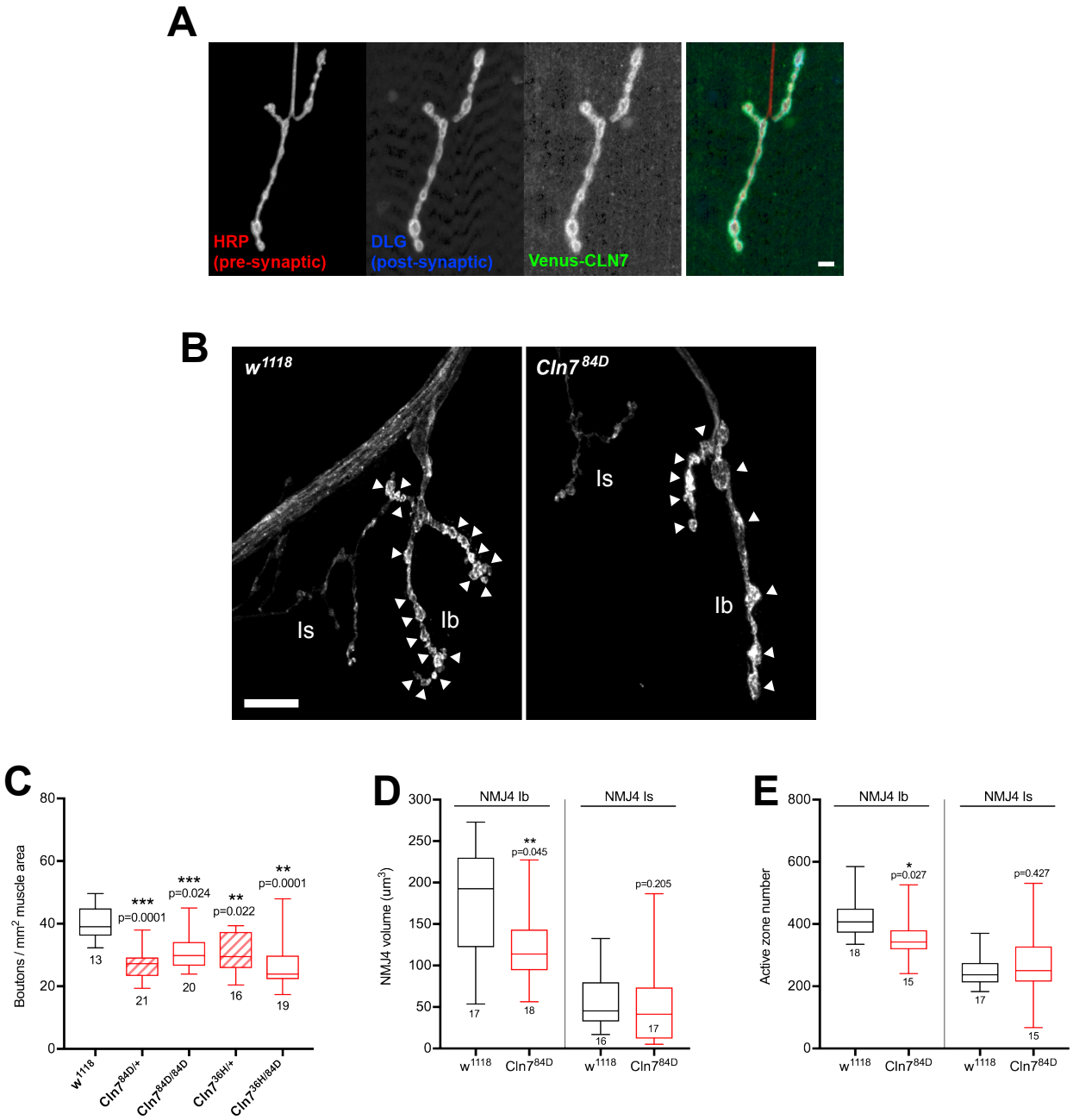


**Figure 2. *Cln7* mutants display underdevelopment of the neuromuscular junction**

A. Localisation of a Venus-Cln7 knock-in reporter protein to the post-synaptic side of the larval neuromuscular junction (NMJ). Late-larval were fixed and labelled to visualise the neuronal membrane (anti-HRP, red), the post-synaptic density (anti-DLG, blue) and Venus-Cln7 localization (anti-GFP, green). Venus-Cln7 co-localises with DLG. Scale bar = 10 μm.

B. Visualisation of NMJs in control $w^{1118}$ and $Cln7^{84D}$ larvae were stained with anti-HRP to visualize the pre-synaptic membrane. Muscle 4 is innervated by phasic type Ib and tonic type Is NMJs. Typical swellings known as boutons are indicated with arrowheads in the type Ib NMJ. The smaller type Is stains less strongly with anti-HRP and the boutons are less distinct. Boutons in *Cln7* mutant type Ib NMJs are fewer but occasionally with a swollen morphology. Scale bar = 10 μm

C. Boutons at NMJ4b were manually counted in $w^{1118}$ control, *Cln7* heterozygote and *Cln7* homozygous mutant lines and normalised to muscle size. Two independent alleles of *Cln7* , 36H and 84D, are both haploinsufficient. A transherozygote $Cln7^{36H/84D}$ alleleic combination has a similar reduction in growth to homoyzgous $Cln7^{84D}$ larvae ANOVA with Dunnett's comparison to $w^{1118}$.

D. Active zone number identified by staining with anti-Brp is significantly reduced in Ib NMJs, concomitant with the reduction in volume, but not in the Is junctions. (2-tailed t-test).

E. Non-subjective measurement of NMJ pre-synaptic volume from rendered confocal z-stacks. The tonic type Ib NMJ is significantly reduced in volume in *Cln7* mutants but the phasic Is junction is not affected (2-tailed t-test).

# Figure 3

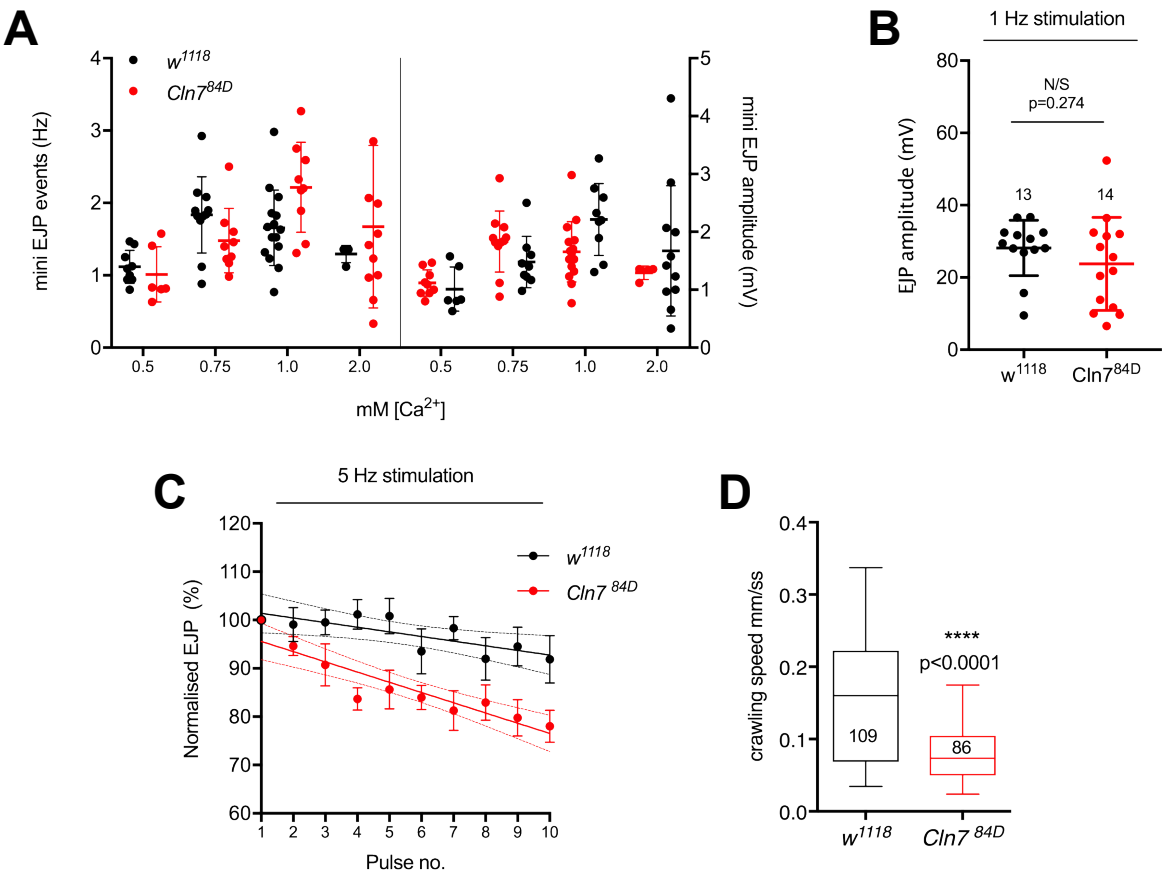


**Figure 3. Functional consequences of loss of Cln7 activity.**

Recordings are shown from muscle 4 in $w^{1118}$ control and *CLN7* $^{84D}$ larvae.

A. The frequency (A) and amplitude (B) of minitaure excitatory junction potentials (mEJP) are not signficantly changed in *Cln7* $^{84D}$ larvae. mEJP frequency (left) was calculated over 120 s for each larva and amplitude (right) from 201-835 events using four different concentrations of extraceullular calcium. Mean is indicated by a solid bar; error bars indicate SD. 2-way ANVOA with Sidak's multiple comparisons was used to assess the effect of genotype. F = 0.6086; DFn = 1; DFd = 66; p=0.4381 for both.

B. Excitatory junction potentials (EJPs) are unchanged in *Cln7* $^{84D}$ larvae. The mean of 16 EJPs at 1 Hz was calculated from n=13 ($w^{1118}$ ) or 14 (*Cln7* $^{84D}$) in 1 mM $Ca^{2+}$. Mean is indicated by a solid line; error bars show SD. p=0.274; Mann-Whitney.

C. Cln7 mutant synapses display an increased rate of fatigue at 5 Hz stimulation. EJP amplitude at 5 Hz was normalised to the mean amplitude at 1 Hz stimulation immediately beforehand. n=4 NMJs for $w^{1118}$ or 6 for *Cln7* $^{84D}$ . Trend lines fitted by linear regression are shown using solid lines with 95% confidence intervals indicated by dashes. $R^2$: $w^{1118}$ = 0.149; Cln7 $^{84D}$ = 0.383. The slopes are significantly different: F = 4.786; DFn = 1; DFd = 96; p=0.0311, t-test.

D. Crawling speed is reduced in *Cln7* $^{84D}$ larvae. Mean speed of $w^{1118}$ control (n=109) and *Cln7* $^{84D}$ (n=86) larvae was determined at 2.5 fps over 5 mins. **** p<0.0001; Mann-Whitney.

# Figure 4

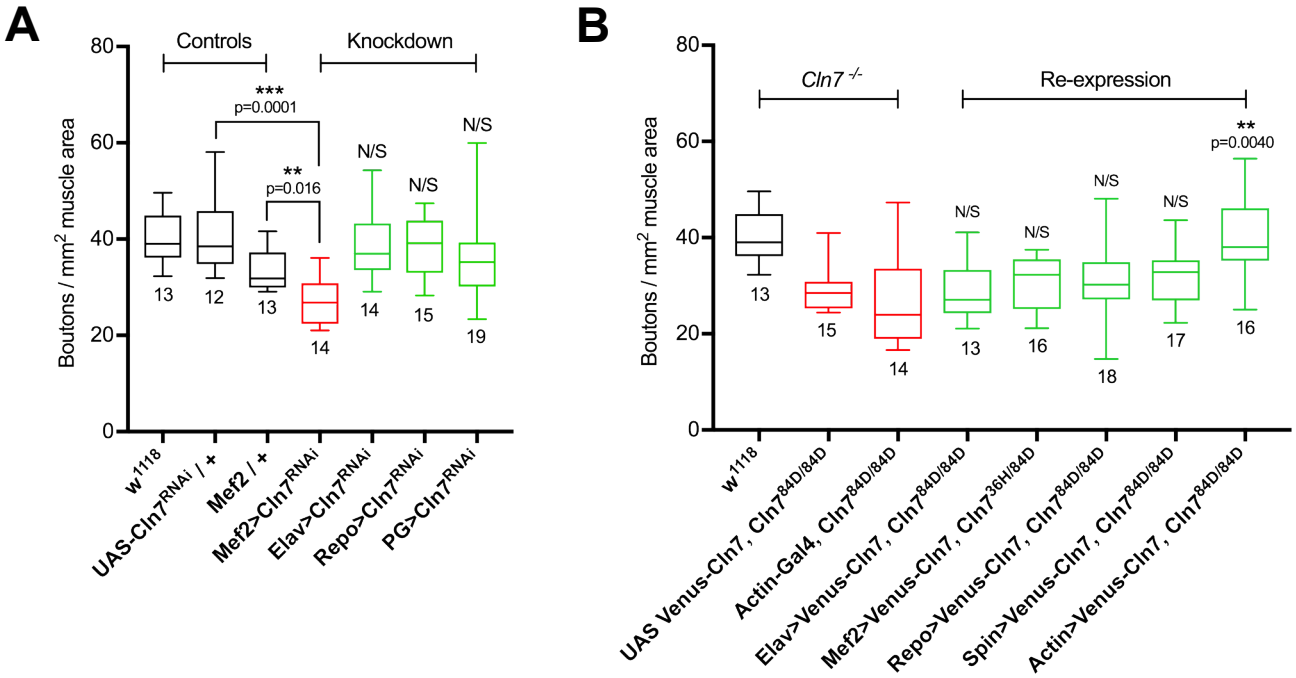


**Figure 4. The cell-type specific requirements for Cln7**

A. UAS-RNAi targeting Cln7 was expressed pre-synaptically in neurons (Elav-Gal4), post-synaptically in muscles (Mef2-Gal4), in glia (Repo-Gal4) or in perineurial glia only (PG-Gal4). Only muscle knockdown resulted in significant decrease in NMJ size. Boutons in $w^{1118}$ are shown for illustration.

B. UAS-VenusCln7 was re-expressed in a *Cln7* mutant background in neurons (driven by Elav-Gal4), muscles (Mef2-Gal4), both neurons and muscles (Spin-Gal4), in glia (Repo-Gal4) or ubiquitously (Actin-Gal4). Only ubiquitously re-expression was sufficient to rescue the underdevelopment phenotype.

ANOVA with Dunnett's comparisons. Min-max plotws of bouton number normalised to muscle surface area. n is indicated. N/S = p>0.05

# Figure 5

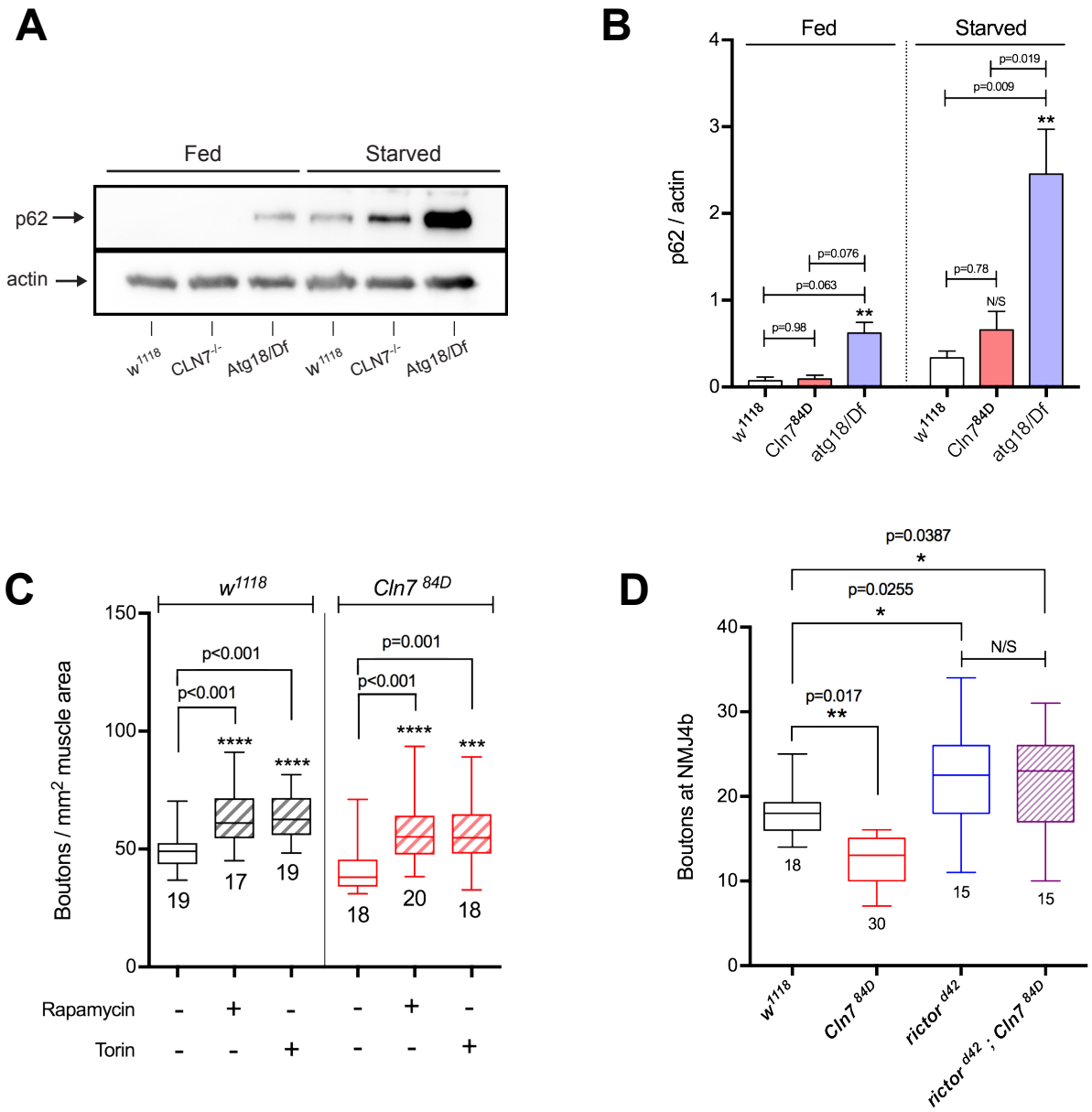


**Figure 5. Autophagy flux proceeds in *Cln7* mutants.**

A, B. The lysosomal substate, p62, does not accumulate in control of *Cln7*$^{84D}$ larvae when feeding but does in *atg18* mutants. A. After 4 hrs starvation, p62 accumulates in control animals. Accumulation is slightly but not significantly increased in *Cln7*$^{84D}$ larvae. In contrast, p62 accumulates to very high levels in starved *atg18* mutants. B. Quantification of A. Bars show mean +/- SEM of p62 band intensity normalised to actin, n=3 for each. ** p<0.01, ANOVA.

C. Inhibition of TORC1 with Rapamycin or Torin drives NMJ overgrowth by increasing autophagic flux. *Cln7*$^{84D}$ larvae respond similarly to control *w*$^{1118}$ larvae suggesting no block in autophagy. Min-Max plots shown with n indicated for each condition. *** p=0.01; **** p<0.001, ANOVA with Dunnett's post-hoc tests.

D. The TORC2-dependent pathway regulating of NMJ development acts genetically downstream of *Cln7*. Mutations in *rictor* drive NMJ overgrowth. In a *rictor/Cln7* double mutant the NMJs display an overgrowth phenotype. This is consistent with Cln7 acting in the post-synaptic cell but Rictor restricting growth pre-synaptically in the neuron. n is indicated for each condition. * p<0.05; ** p<0.01; ANOVA with Dunnett's post-hoc tests.

# Figure 6

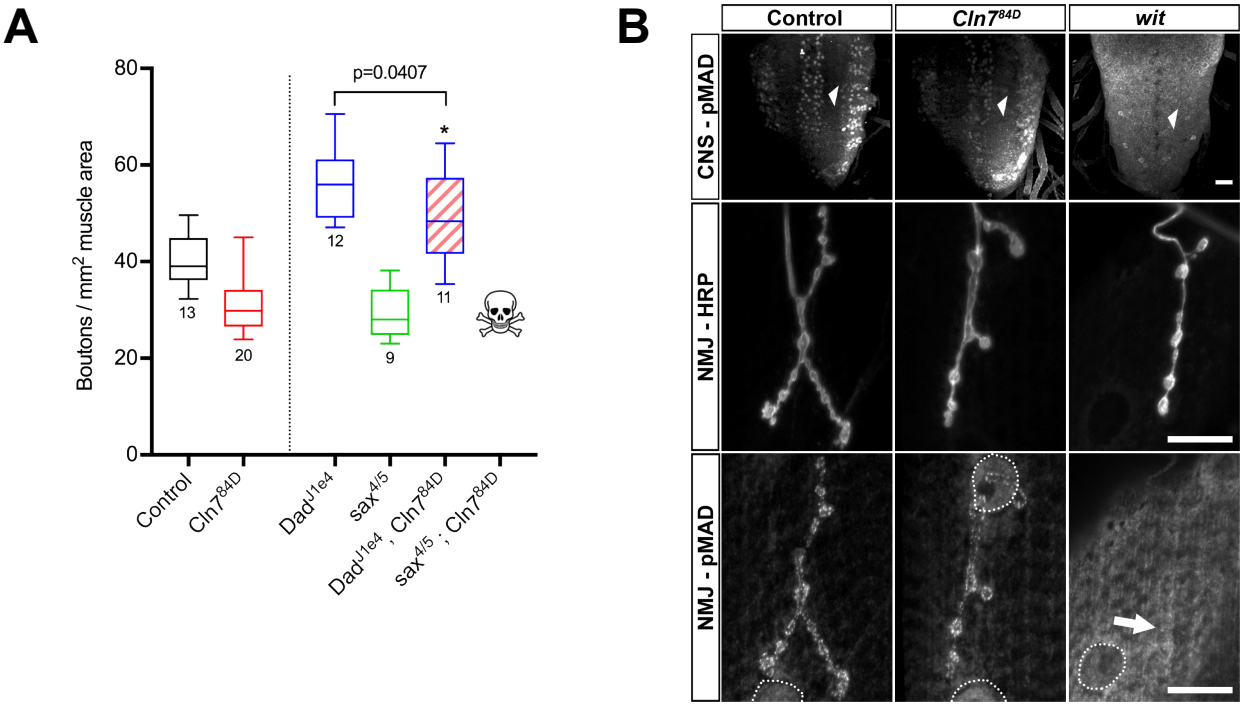


**Figure 6. Retrograde BMP signaling is normal in *Cln7* mutants**

A. Mutations affecting retrograde signaling from the muscle alter neural development. Mutations in the inhibitory SMAD, Dad, drive overgrowth of the NMJ; mutations in the saxophone type I TGFβ receptor result in underdevelopment at a similar level to *Cln7*$^{84D}$ mutants. A double *Dad;Cln7* mutant shows small but signficant moderation of the *Dad* phenotype (2-tailed t-test: t=2.181, Df=21, p=0.0407). A *sax;Cln7* double mutant is lethal early in development. Min-Max plots shown. Control *w*$^{1118}$ and *Cln7*$^{84D}$ data from Fig.3 are included for comparison.

B. Mad is phosphorylated after binding of the Gbb ligand to Tkv, Sax and Wit receptors in the neuron. Characteristic pMad staining is clearly visible in columns of motor neurons in *w*$^{1118}$ and *Cln7*$^{84D}$ CNS but is absent in a *wit* mutant CNS (anti-pMad, top row, arrowheads). pMad staining in boutons is also present in boutons in control and *Cln7*$^{84D}$ NMJs but absent in a *wit* mutant (anti-pMad, bottom column; anti-HRP marks the neuronal plasma membrane, middle column). Similarly, pMad is localised within muscle nuclei but absent in *wit* mutants (dashed circles). Scale bar = 20 μM.

Figure 7

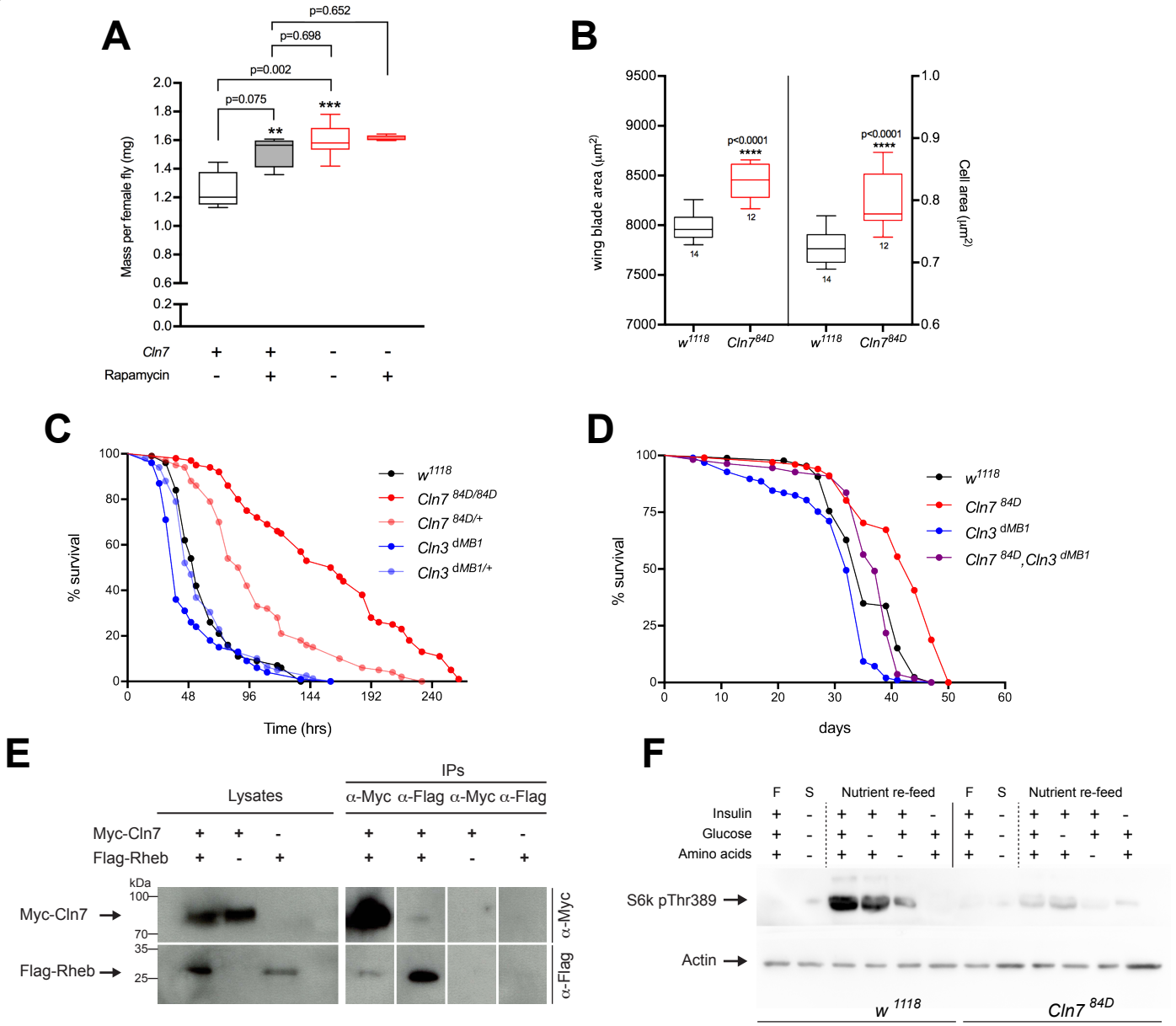


**Figure 7. Cln7 is required for TORC activation**

A. *Cln7*$^{84D}$ flies are significantly larger than isogenic *w*$^{1118}$ controls. Mix-Max plots of mean mass of adult female flies is shown. Development from 1st instar larval stage onwards in food supplemented with the TORC1 inhibitor Rapamycin increases size of *w*$^{1118}$ flies to the same size as the *Cln7*$^{84D}$ flies. Rapamycin does not further increase the size of *Cln7*$^{84D}$ flies. ** p<0.01; *** p<0.001, ANOVA with Dunnett's post-hoc tests. n= 3 repeats of 100 flies weighed in cohorts of 20.

B. Increased size of wings in *Cln7*$^{84D}$ flies is due to increased cell size not increased cell number. *** p<0.001, 2-tailed t-test.

C. Survival of adult flies exposed to 10 mM paraquat. Homozygous or heterozygous *Cln7* mutations confer signficant resistance to paraquat when compared to *w*$^{1118}$ control flies (both p<0.0001, Log-Rank). In contrast, homozygous mutations in a second NCL gene, *Cln3*, are more sensitive to paraquat (p=0.0011). Heterozygous *Cln3* mutants are similar to controls (p=0.84).

D. *Cln7*$^{84D}$ flies show increased lifespan when compared to an isogenic *w*$^{1118}$ control line (p<0.0001, Log Rank). In contrast *Cln3* mutants showed shortened lifespan (p=0.0004). A *Cln7*$^{84D}$*,Cln3*$^{\Delta MB1}$ double mutant has an intermediate lifespan.

E. Cln7 can be immunoprecipitated in a complex with the TOR activating protein, Rheb. Myc-tagged Cln7 and Flag-tagged Rheb were expressed in S2 cells.

F. Phopshorylation of p70 S6K at Ser389 is dramatically reduced in mouse embryonic fibroblasts derived from a *Cln7* mutant mouse. Cells were starved in EBBS for 24 hrs then full nutrients replaced or nutrients minus glucose, amino acids or insulin then cells lysed after 15 mins. F: basal growth conditions; S: starved.